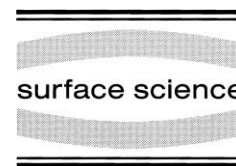




ELSEVIER

Surface Science 407 (1998) 90–103



Structural phase transformation under reversed strain: a comparative study of iron ultrathin film growth on nickel and copper (100)

J. Shen *, C. Schmidhals, J. Woltersdorf, J. Kirschner

Max-Planck-Institut für Mikrostrukturphysik, Weinberg 2, 06120 Halle, Germany

Received 27 October 1997; accepted for publication 11 February 1998

Abstract

The lattice rearrangement processes of the fcc→bcc phase transformation in ultrathin iron films depend on the sign of the applied epitaxial strain. Pseudomorphic iron films grown on nickel and copper (100) substrates are under about 1% strain, which is compressive in the case of Ni and tensile in the case of Cu. The phase transformation in the iron/copper films starts by forming misfit dislocation-like ridge structures oriented along $\langle 011 \rangle$ directions at about 4.6 ML, which soon develop into bcc phase precipitations with indications of a Pitsch orientation. No such dislocation-like structures have been observed for all growth stages of iron on nickel, where the fcc→bcc transformation starts at 5.5 ML by forming bcc island chains along $\langle 001 \rangle$ directions with a significant misfit accommodating effect. Above 10 ML, the step height of the iron films on nickel increases by 11% to about 2.1 Å as a consequence of the fcc→bcc transformation. The drastic differences between the observed transformation phenomena in the two systems are discussed in terms of the specific applied misfit strains and seem to be consistent with former observations of thicker bicrystal systems as well as with continuum theoretical approaches. © 1998 Elsevier Science B.V. All rights reserved.

Keywords: Copper; Iron; Metallic films; Nickel; Scanning tunneling microscopy; Surface thermodynamics

1. Introduction

For nearly one decade, the details of the fcc→bcc phase transformation in ultrathin iron films grown epitaxially on appropriate fcc substrates (Cu, Cu₃Au, Ni) have been of special interest for two reasons. On the one hand, such studies can provide new insights into the atomic reorientation mechanisms and the driving forces of these processes, especially into the first steps of martensitic transformation and their nucleation. On the other hand,

the special magnetic properties of such thin film systems render them candidates for novel 2D magnetic devices, e.g. storage media. These properties are striking and depend dramatically on the film thickness, which is a consequence of (1) the reduced dimensionality of the magnetic system and (2) the morphological and structural peculiarities resulting from the superposition of interface, surface and transformation effects in the course of the film growth.

The background of these efforts is the possibility, by pseudomorphic epitaxial growth, of stabilizing the Fe fcc phase at room temperature, which otherwise exists only above 1183 K and cannot be retained on quenching. Copper (100) has been

* Corresponding author. Fax: (+49) 345 5511 223;
e-mail: shen@mpi-halle.mpg.de

a first suitable substrate. The misfit of -1.1% is small enough to enable complete pseudomorphism for the first monolayers, and its sign enforces an increased lattice spacing that may stabilize a ferromagnetic ground state in the otherwise antiferromagnetic fcc Fe [1].

First extensive experimental investigations of the Fe/Cu(100) system [2–5] revealed a very complicated growth mode, which can be described as a sequence of three distinct stages, as indicated by the results of area-integrating methods as MEED [6], RHEED [7], helium beam scattering [8,9] and low energy ion-scattering [5].

Stage I starts with a Volmer–Weber like growth mode at low coverages and room temperature, characterized by high nucleation density and multi-layer island structures, followed by a gradual switching to the Frank–Van der Merwe mode at almost 3-ML-thick iron film. The structural characterization indicates that the films are tetragonally distorted (vertical expansion) and have a buckled structure in both vertical and lateral directions.

In stage II, at higher coverages, the film seems to grow epitaxially in a nearly pseudomorphic manner: LEED results [4] indicate that the in-plane lattice constant of the iron film is that of the Cu(100) substrate, and the interplanar spacing is slightly contracted, corresponding to a transition of the face centred tetragonal unit cell to a cubic one.

Stage III comprises the phenomena of structural disorder and rearrangement, which are connected with the formation of a bcc equilibrium lattice. MEED results [10] and first real space data [10–13] gave indications for the starting point of this stage to be in the range of 10–21 ML (depending on the carbon content). The existence of bcc precipitates [10] was observed as well as a parent/product phase mixture resulting from a martensitic fcc→bcc transformation [11,12].

In more recent papers [14,15], we followed this transformation across its full range by STM topographs, describing in detail the evolution of the structural transformation stages reflected in the reliefs of particular surface areas, depending on film thickness [14] and temperature, correlated with magnetic properties [15]. It turned out that the system is unstable toward a structural

rearrangement at coverages as low as 4.6 ML. The transformation is initiated by the formation of dislocation-like thin elongated ridges that later transform into a very complicated system of bcc precipitates.

The unexpected complexity of the lattice rearrangement processes influenced by the interplay of misfit accommodation mechanisms and phase transformation phenomena suggests the idea of studying the effect of a variation of the driving forces at otherwise comparable conditions.

It is evident (e.g. cf. Refs. [10,14,16]) that the disorder phenomena of stage III are caused by the inherent instability of the fcc iron film on Cu(100). Due to the lattice mismatch between fcc iron and copper, the film is strained homogeneously, and therefore, a continued pseudomorphic growth increases the deformation energy stored in the overlayer. At a certain critical thickness, this energy can be relieved by the formation of a dislocation network.

A second destabilizing factor is the large difference of nearly 18 meV atom^{-1} [17] in the total energies of the bcc and fcc iron phases, which is responsible for the bcc structure being stable up to 1183 K.

To investigate the influence of the lattice mismatch between fcc Fe and the substrate, and to study the way in which a given stress state will control the transformation, we compare the growth modes of iron films on copper and on nickel substrates, which have the same lattice geometries and rather similar absolute values of the misfit but with opposite signs ($m_{\text{Fe-Cu}} = -1.1\%$; $m_{\text{Fe-Ni}} = +1.3\%$). Thus, iron is under tensile stress on the copper substrate and under compressive stress on the nickel substrate.

In the next section, the experimental details are described, and then, for the first time, we report on in-situ STM observations of iron thin film growth on nickel (100) substrates. The results are presented in comparison with layer growth on copper (100) at the same number of monolayers. In order to bring the results into the context of transformation phenomena under applied stresses, some theoretical concepts are summarized in Sections 4 and 5, followed by a detailed discussion of the observations in Section 6.

2. Experimental details

The experiments were performed in an ultra-high vacuum (UHV) system equipped with STM and cylindrical mirror analyzer (CMA) based Auger electron spectroscopy (AES). The base pressure of the UHV system was better than 7×10^{-11} mbar. Prior to film deposition, the copper and nickel substrates were treated by somewhat different preparation procedures. The copper (100) substrate (miscut $< 0.5^\circ$) was prepared by low-energy ion sputtering (Ne, 300 eV) at 870 K, followed by controlled linear cooling to 790 K and natural cooling to room temperature. The resultant surface was contamination-free within the detection limits of the AES, and had large atomically flat terraces with a typical width of several hundred nanometers. The nickel substrate cut to within 0.3° of the (100) plane was initially cleaned by cycles of Ar^+ sputtering at 500 eV at 800 K. This procedure generally leads to a carbon contamination level of the substrate of 10% of a monolayer. The sample was then annealed at 800 K in an O_2 atmosphere with a partial pressure of about 1×10^{-8} mbar for 20 min. The O_2 was subsequently pumped away, leaving the substrate to be further annealed in UHV at 800 K for 5 min. This preparation procedure yields an AES clean Ni substrate with a typical terrace width in the order of 50–100 nm.

The iron films were deposited from an iron wire (5 N in purity) heated by e-beam bombardment. All films were grown at room temperature with deposition rates of less than 0.3 ML min^{-1} . The pressure never exceeded 2×10^{-10} mbar during the Fe evaporation, which guarantees the contamination of C and O in the films to be below 1 at.-%.

The deposition of Fe was carried out inside the STM sample stage, with an incident angle of about 15° with respect to the surface. The STM tip was withdrawn about $1 \mu\text{m}$ away from the surface during deposition to avoid any possible shadowing effect of the tip. The deposition was frequently interrupted to allow the STM images to be taken in small incremental steps of thickness. The present STM is custom-designed [18] and allows us to repeatedly scan the same surface area while increasing the film thickness. This also provides a

highly reliable way of determining the coverage by directly counting the distribution of iron in all monatomic layers.

All STM images were taken in the constant current mode at a tunneling voltage of 1 V and a tunneling current of 0.1 nA. From time to time, tunneling parameters were varied in order to check for any apparent changes in the images, but in no case were any parameter dependent features observed.

3. STM observations of phase transformation

The growth of both Fe/Cu(100) and Fe/Ni(100) proceeds in a layer-by-layer manner for the first several layers. For both systems, we acquired series of STM images following the growth at the same surface location until the films have completely transformed from an initial fcc-like into a bcc structure. As the focus of the present paper is the fcc→bcc phase transformation, in the following, we will concentrate on the growth stages that are closely related to the transformation while omitting the initial stages of growth. Fig. 1 shows the typical STM morphology of 5.6 ML (a) and 6.2 ML (c) Fe/Cu(100) films in the left column, and the Fe/Ni(100) films with the corresponding thickness in the right column (b and d). It is immediately evident that at 5.6 ML, the Fe/Cu film has a good layer-by-layer morphology that is characterized by the presence of merely two exposed layers. The 5.6 ML Fe/Ni film indicates a slight deviation from a good layer-by-layer growth, as evidenced by the presence of a small amount of seventh-layer nuclei (bright in contrast). The main difference between the morphology of the Fe/Cu(100) and the Fe/Ni(100) films at this stage is the island size. The islands of the Fe/Cu(100) are typically at least 10 times larger than those of the Fe/Ni(100) film, indicating that the Fe/Ni(100) system has a higher nucleation density. The shape of the islands in both systems is rather irregular without exhibiting a clear preferential edge orientation.

A further increase in thickness to 6.2 ML causes the Fe/Cu(100) system to start a complicated structural transformation process, which could be identified as a martensitic path with the bcc(110)

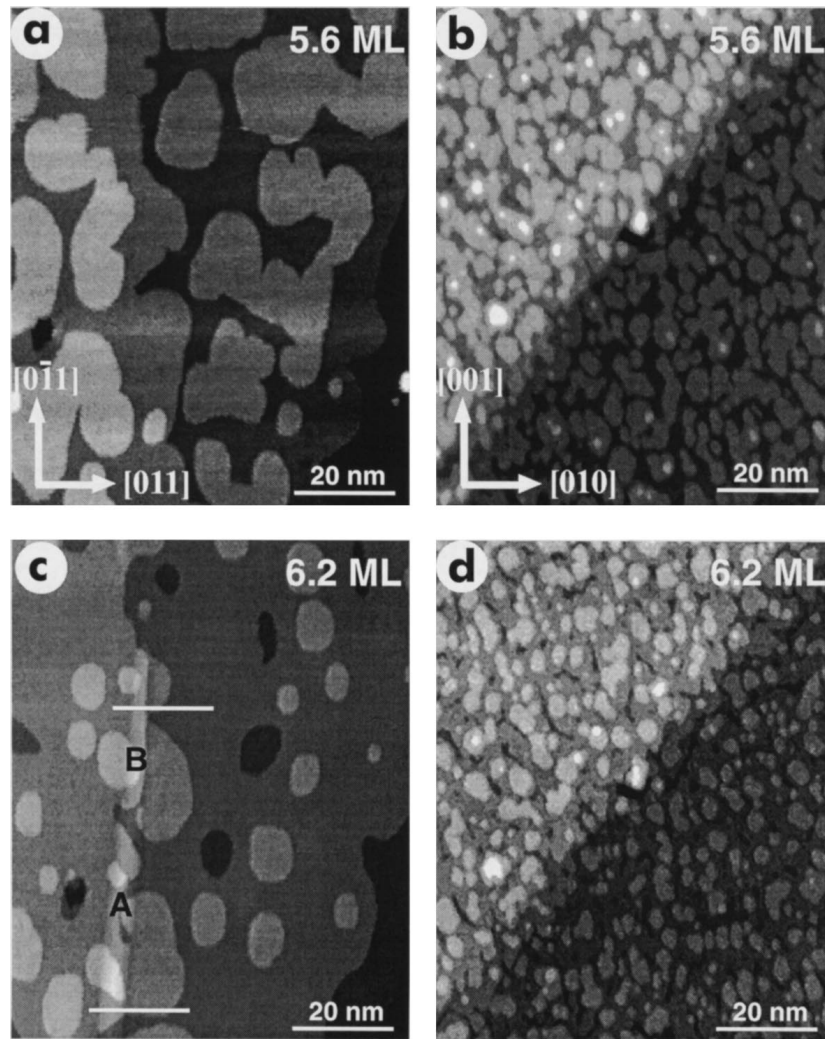


Fig. 1. STM topography images of Fe/Cu(100) (left column) and Fe/Ni(100) films (right column). The island density of the Fe films on Ni is significantly higher than that of the Fe films on Cu. At 6.2 ML, a ridge-like structure appears on the surface. The marked “A” and “B” structures will later follow different paths to develop into bcc(110) structure.

structure as the final product [14]. At 6.2 ML (Fig. 1c), a ridge-like structure appears along the monoatomic step inherited from the substrate, which possibly represents the early stage of a misfit dislocation. It is worthwhile noting that the nucleus and early stages of a dislocation can be considered as pre-defects that are involved in the starting phase of a martensitic transformation (see Section 6). The overall axis of this elongated structure is nearly parallel to the $[0\bar{1}1]$ direction of the underlying substrate (deviation 3°). The trans-

forming region consists of two parts, A and B, whose line profiles exhibit different characteristics as shown in Fig. 2. Evidently, along the lines indicated in Fig. 1c, feature A has an almost symmetric buckled structure, whereas feature B has slightly tilted planes on one side that emerges smoothly from the surrounding fcc area, and a sharper drop on the other side to a small groove whose depth is on the order of 20% of the fcc step height. The tilting angle of the B plane is about 3° with respect to the fcc (100) surface. At this stage,

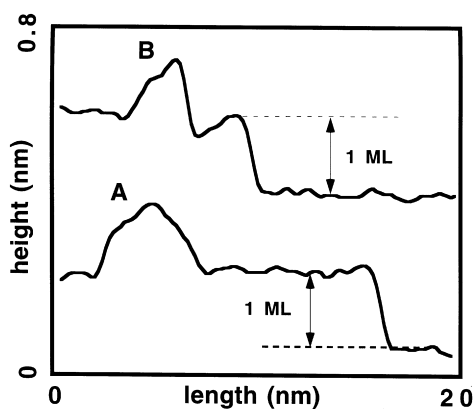


Fig. 2. Profiles of the marked white lines in Fig. 1c showing the different characteristic features of structures "A" and "B". Feature "A" has a symmetric shape, whereas feature "B" emerges smoothly on one side but drops rather abruptly on the other side leaving a groove in between "B" and the surroundings.

A and B represent just initial steps of the lattice rearrangement process and do not show any characteristic features of a well-transformed bcc structure.

Such ridge-like structures are not visible in the Fe/Ni(100) film at 6.2 ML. The surface of the film consists of four exposed layers, and thus it is somewhat rougher than the 5.6 ML film. We will demonstrate later in Fig. 4 that starting from 6 ML on the growth mode of the Fe/Ni films changes from a layer-by-layer to a multilayer one.

Going up to 7.9 ML, the transformation in the Fe/Cu(100) film proceeds further as evidenced by the major structural change of the features A and B. As shown in the top-left of Fig. 3, the features have developed into a flat-topped parallelogram-shaped island separated from the surrounding area by shallow grooves. The shear angle between the parallelogram is close to the angle between the $\langle 111 \rangle$ and $\langle 001 \rangle$ directions in the bcc(110) plane (55°). Meanwhile, another B-type of structure, C, emerges along a nearly exact [011] direction. At a later stage of the transformation (10.2 ML, bottom left), the parallelogram-shaped A and B consist of several layers with an interlayer distance clearly larger than that of the non-transformed surrounding area. The histogram measurement [14] indicates that the interlayer distance of the transformed

region is about 2.0 \AA , a value that is very close to that of the bcc(110) interlayer distance. Structure C has developed into a pile of tilted planes with still one side to be smoothly connected with the fcc region. The structure of all these transformed regions is significantly out of the registry of the surrounding fcc Fe layers in both the lateral and vertical direction, strongly suggesting that the major transformation process occurs between 7.9 and 10.2 ML.

At similar thicknesses, the Fe/Ni(100) system also experiences morphological changes, but in a much less dramatic way. The morphological changes, on the relatively small scale in Fig. 3, are mainly viewed as a significantly increasing surface roughness. The number of exposed layers amounts to five at 7.9 ML and six at 10.2 ML. The change in surface roughness is quantitatively shown in Fig. 4, which displays the root-mean-square (rms) roughness as a function of the thickness. Oscillations with a period of 1 ML are clearly visible up to 6 ML. Within each oscillation, the roughness hits a maximum at the half integral number of layers and reaches a minimum at the completion of each layer. These features are typical signs for a quasi-layer-by-layer mode. Above 6 ML, the roughness starts to increase almost linearly with hardly any oscillations. The increase in the rms values reflects the increasingly rough surface morphology of the films as shown in Figs. 1d and 3b,d.

The transformation of the Fe/Cu(100) system, in the particular scanning area shown above, seems to be completed around 11 ML. Fig. 5 demonstrates the final stages of transformation (10.7 ML (a) and 11.5 ML (b)). In the 10.7 ML image, the transformed structure covers three-quarters of the whole area except the bottom-right part. With additional 0.8 ML coverage of Fe, the remaining area is also converted into the bcc structure (11.5 ML image).

For the Fe/Ni(100) films, the topography images at these thicknesses only indicate a further increase of roughness. However, the average step height of the exposed layers, as measured by the STM histogram analysis, is distinctly larger than that of the films below 10 ML. As shown in Fig. 6, below 10 ML, the average step height is around 1.9 \AA ,

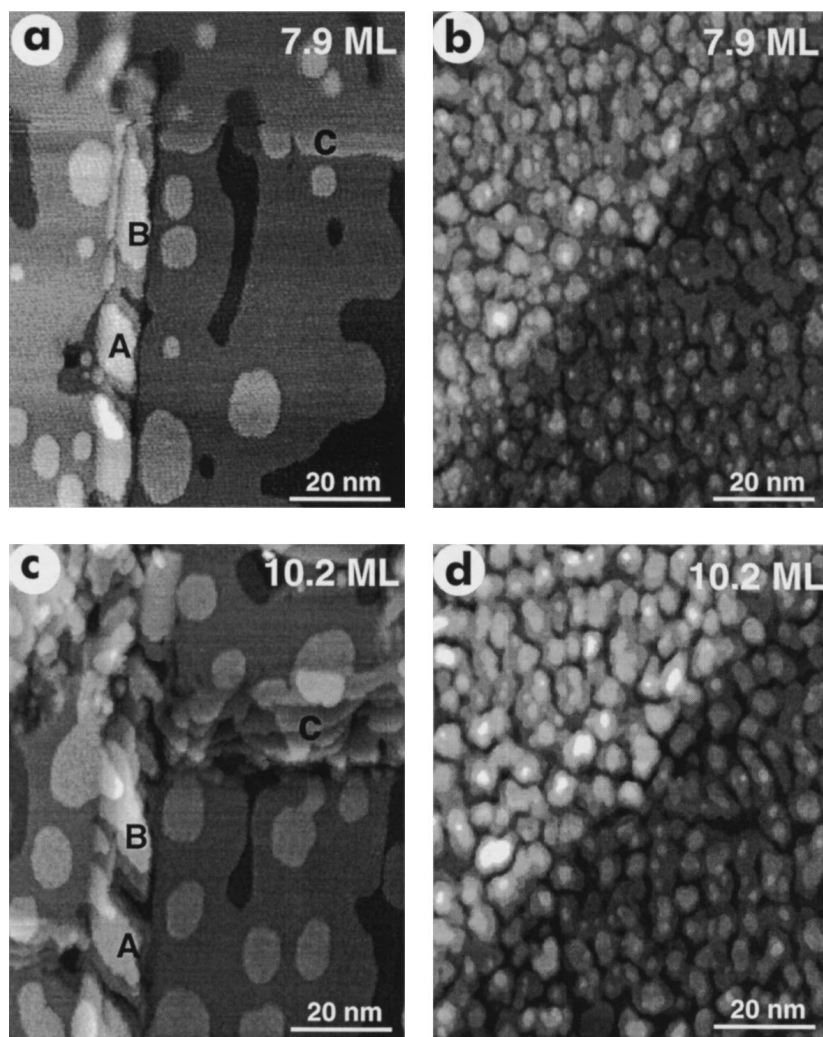


Fig. 3. STM topography images of Fe/Cu(100) (left column) and Fe/Ni(100) films (right column). Note the images of the Fe/Cu and Fe/Ni films were recorded from the same surface locations as those in Fig. 1, respectively. At 7.9 ML, a new feature “C” appears nearly perpendicular to the original ridge-like structure. “A” and “B” become disconnected with clear signs of shear mechanism involved. The changes of the Fe/Ni films, from the topography, are only viewed as increasing roughness.

which is larger than the expected bulk fcc Fe(100) interlayer distance ($\sim 1.8 \text{ \AA}$) as well as the measured step height of the Ni substrate ($\sim 1.7 \text{ \AA}$). The vertical expansion of the interlayer spacing of the Fe films can be interpreted as a Poisson-like response to the lateral compression of the Fe films. Any strain relief mechanism should therefore lead to a decrease of the interlayer distance. However, Fig. 6 clearly indicates that above 10 ML, the step height of the Fe/Ni(100) films increases by 11%

to about 2.1 \AA . This change of the step height should be quite reliable since the data were measured from the same surface area under the same scanning conditions. Therefore, such a sudden further increase of the step height has to be associated with the structural transformation from fcc(100) to bcc(110). In this case, the enormous increase in interlayer distance is completely consistent with the emerging understanding of the misfit accommodating the transformation processes pre-

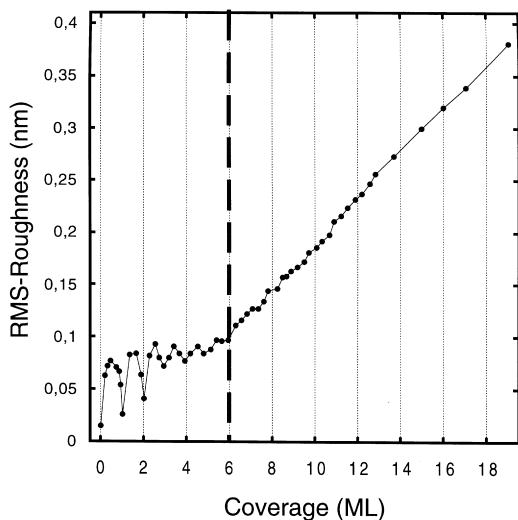


Fig. 4. Surface roughness (rms) as a function of thickness of the Fe/Ni films. Oscillations corresponding to layer-by-layer growth are clearly visible below 6 ML. Above 6 ML, the roughness increases rapidly without oscillations, in agreement with the multilayer morphology of the films at higher thicknesses in Fig. 3.

sented in Section 6. The LEED pattern acquired from films above 10 ML (inset picture in Fig. 6) shows a “ 3×1 ”, which has been discussed as four bcc(110) domains [4]. We also notice that a previous LEED study [19] has also produced evidence that the Fe/Ni system contains a certain amount of the bcc phase at 10 ML, which qualitatively agrees with our observations.

Additional information on the fcc \rightarrow bcc transformation process can be found by examining the film morphology on a larger scale. Fig. 7 shows the morphology of a 10.7 ML Fe/Cu(100) film (a) and Fe/Ni(100) film (b) with a scanning area of $400 \times 400 \text{ nm}^2$. A large number of ridge-like structures in the Fe/Cu film form $\langle 011 \rangle$ -oriented misfit dislocations in a network-like arrangement. As mentioned earlier (Fig. 3), at 10.7 ML, the network lines simultaneously represent the transformed bcc structure. The area between the network lines is covered by a still untransformed fcc material, whose morphology is clearly distinguishable from the bcc network lines. According to our STM measurements, almost the whole film has become bcc-like above 12 ML.

For the Fe/Ni film in Fig. 7, a feature that is not apparent in the small area images (Figs. 1 and 3) is clearly visible: some grooves are arranged along $\langle 001 \rangle$ directions and thus also form a network. (We have indicated some of the aligned grooves by white arrows.) In the inset of Fig. 7b, a magnified picture of a groove marked by a white rectangular box is shown. It is clear that the grooves represent just the gaps between two neighboring $\langle 001 \rangle$ -oriented chains of islands.

Unlike in the Fe/Cu case, it is difficult to determine the extent of the transformation in the Fe/Ni films because easily distinguishable features between the transformed and untransformed areas are absent. An observation of relevance may be the density of the grooves, which are displayed as a function of thickness in Fig. 8. The grooves start to appear around 5.5 ML. With increasing thickness, their density rapidly increases and reaches a maximum at about 10 ML. Above 10 ML, their density decreases as the grooves start to be filled randomly by the deposited atoms. We conjecture that the islands that form the chains on both sides of the grooves are of the transformed bcc phase. Their arrangement decorates the sites of preferred nucleation. After exceeding a critical thickness, the pseudomorphic growth of the first iron monolayers will lead to the formation of periodic strain maxima aligned along $\langle 001 \rangle$ directions. The distances of these configurations observed by us amount to 30–40 nm which is in good agreement with the values expected for a misfit of nearly 1%. The lines of maximum strain may act as centers of preferred generation of bcc nuclei. During further growth, the particular geometry of the forming bcc islands is able to completely accommodate the misfit stresses and to make any misfit dislocations unnecessary, as shown in Section 6.

Up to 10 ML, the majority part of the Fe film on Ni(100) has been changed into the bcc structure, and the misfit stress is relieved in the transformed areas. In the absence of the misfit strain field, the groove regions are no longer particular nucleation sites and start to be filled randomly by newly landed Fe atoms. This explains why the density of the grooves has a maximum at 10 ML. This maximum remarkably corresponds to the observed sharp rise of the surface step height at

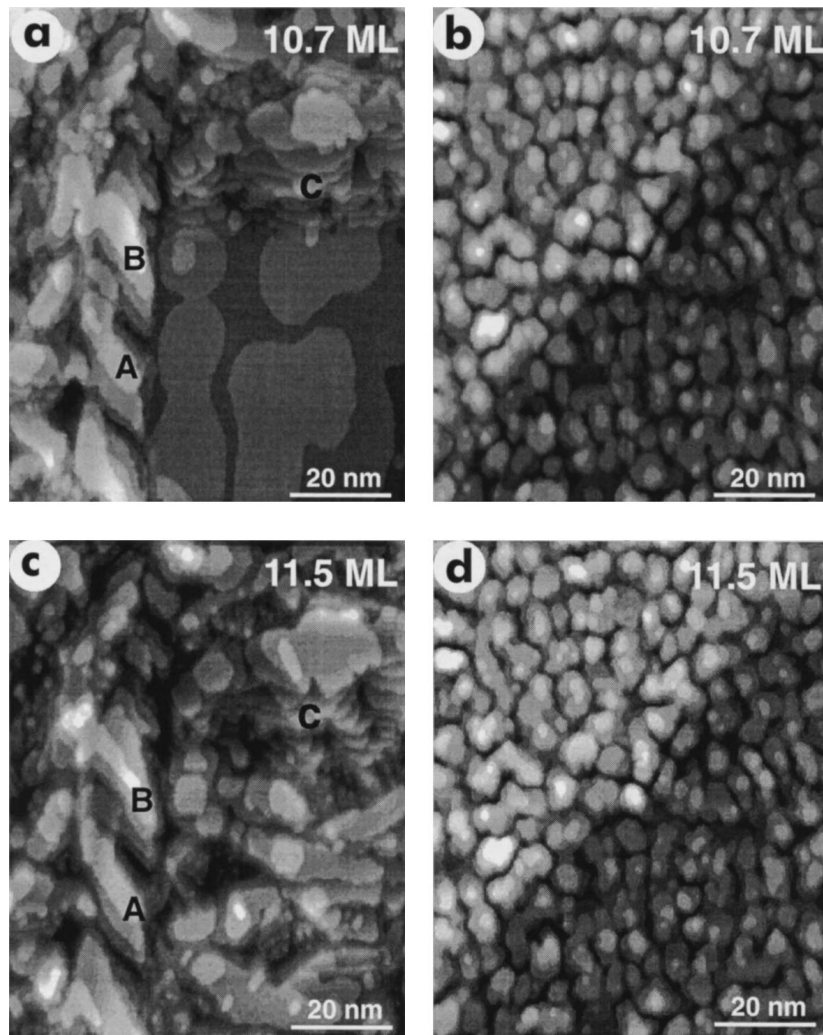


Fig. 5. STM topography images of Fe/Cu(100) (left column) and Fe/Ni(100) films (right column) after sequential deposition of Fe films on to the films in Fig. 3. At 10.7 ML, only the bottom right part remains fcc-like in the Fe/Cu film, which becomes full bcc at 11.5 ML. The Fe/Ni films undergo a distinct increase of the step height above 10 ML, which will be shown in Fig. 6.

10 ML, as demonstrated in Fig. 6. The sharp rise of the groove density above 5 ML (see Fig. 8) suggests that the fcc→bcc phase transformation starts at about 5.5 ML in the Fe/Ni system. This thickness is close to that of the onset of the phase transformation in the Fe/Cu system (4.6 ML; see Ref. [14]), and the speed of the transformation process in the two systems is quite comparable.

We find it quite remarkable that the Fe/Ni system that is under compressive stress opens up

numerous grooves that further increase the open area. Intuitively, one would expect the bcc phase, which has a larger atomic volume, to cover the surface in a more densely packed way, rather than to lead to a less compact film morphology, but this puzzle is resolved in Sections 5 and 6.

In the Fe/Cu system, the fcc→bcc transformation also results in a surface roughening in spite of the tensile strain. As clearly shown in Fig. 3c, the transformed bcc regions are significantly

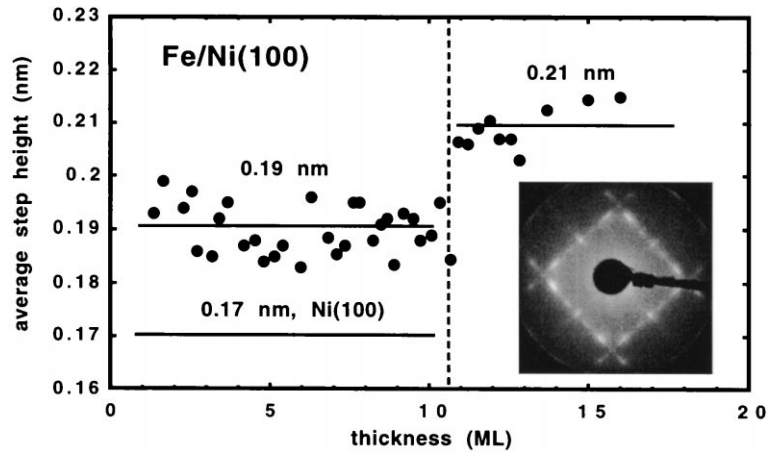


Fig. 6. Step height of the Fe/Ni films as a function of thickness. All data were measured from images taken from the same surface location with the same scanning conditions. The Fe films have a clearly larger step height than that of the Ni substrate. Above 10 ML, the step height sharply rises to a value that is closely correlated with the bcc(110) structure. The inset picture (11 ML taken at 156 eV) shows a typical LEED pattern of the films above 10 ML.

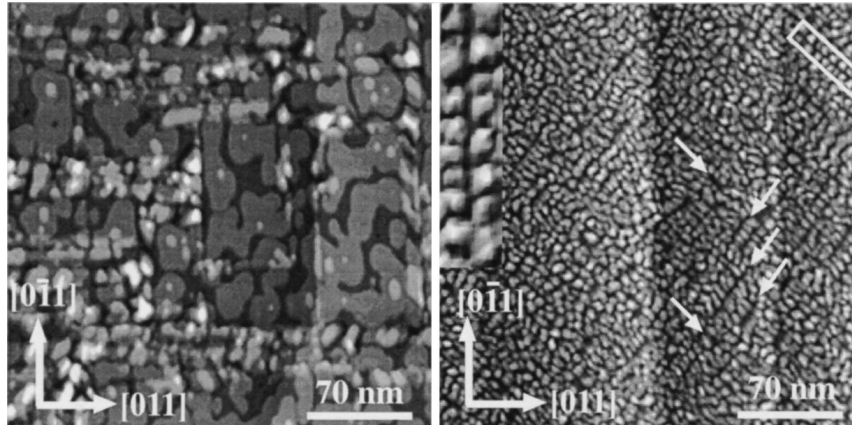


Fig. 7. STM topography images of 10.7 ML Fe/Cu(100) (left) and Fe/Ni(100) films (right). On a relatively large scale, two types of network are visible in the Fe/Cu and Fe/Ni films, respectively. On Cu(100), a network is formed by $\langle 011 \rangle$ oriented ridge-like structures, whereas on Ni(100), it is formed by $\langle 001 \rangle$ -oriented grooves, some of which have been indicated by the white arrows. The inset picture is a magnified image of a particular groove marked by a white box. Clearly, the grooves are formed by chains of islands.

rougher than the fcc regions. Such roughening is likely caused by two reasons: (1) in the bcc region, the atoms are out of the registry of the substrate, and thus the epitaxial relationship no longer holds; and (2) the bcc(110) islands have a high step edge barrier [20] that hinders the interlayer mass transport during further deposition.

4. Influence of stresses on the formation of bcc precipitations

The different transformation behaviour of the iron layers on copper and nickel and most of the observed structural phenomena can be well understood if taking into account (1) the specific possi-

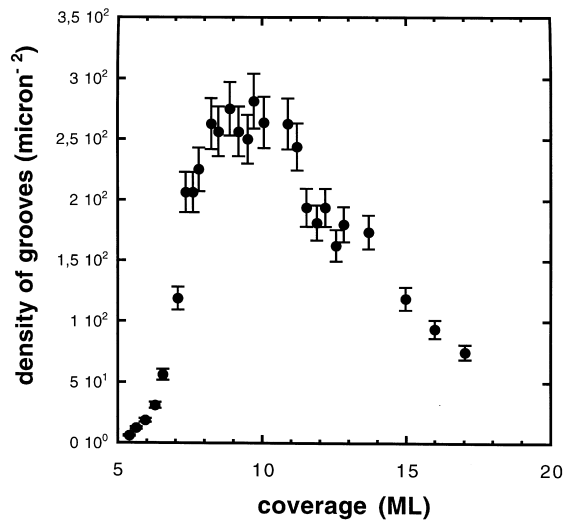


Fig. 8. Density of the grooves in Fe/Ni films as a function of thickness. The grooves start to appear at about 5.5 ML, and reach a maximum at about 10 ML. At a higher thickness, the density decreases because the grooves start to be filled by further deposited Fe atoms.

bilities of misfit accommodation in both systems and (2) the effects of different applied stresses on the bcc precipitation kinetics.

As described in Ref. [14], the formation of these bcc nuclei may be regarded as a first step of a martensitic fcc→bcc transformation because the lattice rearrangement in pure iron is also possible via a diffusionless mechanism as is known for iron–carbon alloys. In this process, the atoms forming the fcc-iron shift abruptly over certain distances along specific directions in order to occupy sites corresponding to the bcc lattice. (The martensitic nature of the phase transformation in pure iron was proved in the case of high cooling rates in Ref. [21], and the formation of Widmannstätten ferrite was also shown to be martensitic [22].)

As several habit planes are possible with partly irrational indices and as different fcc/bcc relationships exist depending on the applied stress [23], the martensitic fcc→bcc transition is structurally not unambiguously pre-determined. Moreover, in the present case of ultrathin film growth, the transformation mechanisms will be influenced by superimposed interface and surface effects and by

the specific growth morphology which is determined by effects of pseudomorphism, misfit strain [24] and possibly generation of misfit dislocations [25].

Important work on the influence of stresses on the formation of bcc precipitations was already done in the late 1960s by Matthews et al. [26–29] who investigated iron films grown under UHV conditions and later transferred in air to an electron microscope. Although the carbon contamination level of the iron films and the substrates was not determined, their results are a helpful base for the interpretation of our findings.

As the bcc regions within the fcc matrix are formed in the presence of stresses in the film plane due to the misfit strain—which is reversed in the pseudomorphic overgrowths on copper and on nickel—the favouring or hindering effects of such applied stresses on the formation of precipitations of different orientations must be considered. Eshelby [30] describes this influence by introducing an effective interaction energy, E_{int} , which represents the change in total formation energy of a precipitate when formed in the matrix under constant load. If ϵ_{ij}^T denotes the transformation strains that homogeneously transform a given fcc region into a bcc precipitation of volume, V , without any applied load, and p_{ij}^A denotes the components of the constant applied stress in the absence of the precipitate, then one has:

$$E_{\text{int}} = - \int_V \sum_i \sum_j p_{ij}^A \epsilon_{ij}^T dV,$$

if the elastic constants of fcc matrix and bcc precipitate are assumed to be equal.

A calculation of values for the present cases as done in Ref. [29] is possible if the p_{ij}^A components are taken to represent the stresses in the completely pseudomorphic strained iron overgrowth and if the ϵ_{ij}^T components are taken as the so-called Bain strains [31] describing the principal strains of the fcc→bcc transformation.

According to electron diffraction studies [26–28], three important orientation relationships between fcc and bcc phases, which are generally known and described in textbooks on the crystallography of martensitic transformations (e.g. cf.

Refs. [23,32,33], are relevant to the Fe/Cu and Fe/Ni systems. These are the Nishiyama [34], the Kurdjumow–Sachs [35] and the Pitsch [36] orientations, characterized by the following relations:

Nishiyama: $\{111\}_{\text{fcc}}$ parallel to $(110)_{\text{bcc}}$ and $\langle\bar{1}10\rangle_{\text{fcc}}$ parallel to $[100]_{\text{bcc}}$,

Kurdjumow–Sachs: $\{111\}_{\text{fcc}}$ parallel to $(110)_{\text{bcc}}$ and $\langle\bar{1}10\rangle_{\text{fcc}}$ parallel to $[\bar{1}11]_{\text{bcc}}$,

Pitsch: $\{100\}_{\text{fcc}}$ parallel to $(\bar{1}10)_{\text{bcc}}$ and $\langle110\rangle_{\text{fcc}}$ parallel to $[112]_{\text{bcc}}$.

The combination of these planes and directions yields the possible 12 Nishiyama, 24 Kurdjumow–Sachs and 12 Pitsch variants of relationships. For these 48 variants, which can be subdivided into eight groups of equivalent crystallography in the film plane, the interaction energy density ϵ_{int} (i.e. the E_{int} value per unit volume) was calculated in Ref. [29] for both the systems Fe/Cu (tension) and Fe/Ni (compression).

It turned out that ϵ_{int} , which can be regarded as the driving force for the formation of the bcc precipitate within the fcc matrix, is strongly orientated and stress-dependent and can provide detailed interpretations of the different phenomena observed in the Fe/Cu and Fe/Ni systems.

The calculated ϵ_{int} values for the eight equivalent groups and the two systems vary between -1.49 and $+1.62$ ergs cm^{-3} , and for those three groups of orientations observed in pseudomorphic thin iron films on copper and on nickel [26–28], these values are negative. In the Fe/Cu system, a group of four Pitsch variants corresponds to the most negative ϵ_{int} value of this system (-1.49 ergs cm^{-3}). In the Fe/Ni system, a group of four other Pitsch variants, different from those observed for iron deposited on copper, corresponds to the most negative ϵ_{int} value of this system (-0.40 ergs cm^{-3}). The findings that not all orientations with negative ϵ_{int} values or not only those with the most negative values were observed are due to the specifics of the corresponding transformation paths. The detailed atomic movement during transformation into a bcc region of given orientation follows a specific path, which can be hindered by the applied stress, although the ϵ_{int} value is negative. Therefore, in Ref. [29], the shear mechanisms for the different orientation relationships were investigated additionally to find out

those particular shear systems on to which the applied stress is resolved. As a result, it could be stated that (1) all bcc precipitate orientations with negative ϵ_{int} values not experimentally observed correspond to shear mechanisms, which were strongly hindered by the misfit stress and (2) that the observed orientations with the most negative ϵ_{int} values, i.e. the different two groups of ever 4 Pitsch variants each for Fe/Cu and Fe/Ni, respectively, correspond to shear mechanisms aided by the misfit stress. Generally, these mechanisms follow a shear system with a $\{110\}$ shear plane and a shear in the $\langle\bar{1}10\rangle$ direction.

5. Discussion

For the iron/copper ultrathin films, our STM observations seem to give an indication of the activation of the Pitsch shear mechanism as can be seen in the characteristic $\langle 011 \rangle$ direction of the ridge patterns in Fig. 7 as well as in the tilted plane region of Fig. 3. Obviously, these features may be only the initiating steps of such rearrangement processes; however, alternative Nishiyama or Kurdjumow–Sachs orientation relationships would involve shear systems with a $\{\bar{2}11\}$ shear plane or a shear in the $\langle\bar{2}11\rangle$ direction, for which we did not find any direct evidence.

In contrast to the iron/copper films, no dislocation-like features have been observed for the iron/nickel films in the whole thickness regime studied (0–20 ML). The absence of dislocations indirectly shows that the bcc islands, i.e. the chain islands along the grooves, are in a particular Pitsch orientation typical for the Fe/Ni system [28]. The formation of such Pitsch-oriented bcc precipitates results in a relief of the compression in the film plane, i.e. a contraction of 7.3% along one of the two $\langle 011 \rangle$ directions in the Fe/Ni interface and a contraction of 1.7% along the other. Therefore, the atomic shift connected with this rearrangement process is a means to completely accommodate the misfit of 1.3% between the nickel substrate and the fcc iron overgrowth. This explains the absence of misfit dislocations in the Fe/Ni system generally observed in the study of Matthews and Jesser [27] as well as in our ultrathin film experiments as

demonstrated in the right hand parts of Figs. 1, 3, 5 and 7. Conclusive evidence for the accommodation of compressive strain by the bcc island formation in this system is the reversal of the sign of the elastic film strain if a sufficient part of the iron is transformed into bcc particles in one of the above-described favourable Pitsch orientations, as was observed in Ref. [27].

A further striking effect of the formation of Pitsch oriented bcc islands in the Fe/Ni system, which is strongly correlated to our ultrathin film observations is the expansion perpendicular to the film plane which accompanies the lattice transformation. This expansion amounts to 13.4% [27], which agrees reasonably well with the experimental value of 11% revealed by our measurements of the step heights on Fe/Ni(100) (see Fig. 6).

Finally, we will briefly discuss the role and possible evidence of dislocations in our ultrathin film systems. In ultrathin specimens of a few monolayers in thickness, the term dislocation can only be used under certain restrictions. Any concept of dislocation classification loses its significance when the core structure dimension is of the same order of magnitude as the thickness of the surrounding material. Moreover, in our cases of epitaxial fcc iron monolayers on copper and nickel substrates, the mutual complex interactions of surface and interface effects, superimposed misfit strains and the starting stage of a transformation will affect the process of dislocation generation in such a way that only further growth will determine the true type of forming dislocation. The nucleation sites of such dislocations and their early stages should be considered as generalized pre-defects, which may be examples of lattice instabilities and imperfections as discussed in the localized soft mode model [37]. In this sense, the ridge-like structures shown in Figs. 1 and 3 seem to be stages of dislocation evolution in the Fe/Cu system. The symmetric dislocation lines are narrow in the initial stages of growth, then changing their morphology quickly as demonstrated in Fig. 5. In iron deposits thicker than 10 ML on copper substrates, dislocation networks were observed in Ref. [26], which accommodate part of the misfit.

The critical film thickness, d_c , for the formation of misfit dislocations can be calculated within

different frameworks of theoretical concepts, depending on the mechanism responsible for their generation. These mechanisms are (1) gliding of grown-in substrate dislocations via a force balance within the strained epitaxial system (which is not valid in our case of nearly dislocation free copper and nickel substrates) and (2) spontaneous generation to reduce the strain energy of the overgrowth (e.g. cf. Refs. [24,25,38]). For the Fe/Cu system, the approximation for the first mechanism predicts $d_c = 5.5$ nm (equivalent to 30 ML fcc-Fe film) in case of complete pseudomorphism (overgrowth is strained to perfect fit). Other models yield nearly 4 and 6 nm (21 and 33 ML, respectively) [26]. For the Fe/Ni system, there are similar amounts of d_c (about 5 nm), assuming that the dislocations have the same geometry as those observed in the Fe/Cu system [27]. Generally, such calculations of d_c are rough approximations as essential parameters of the interface models are unknown or not known with sufficient accuracy, e.g. the strength of interaction, the specific surface state of the substrate and mechanical parameters of the interface. Thus, the occurrence of misfit dislocations at lower film thickness than predicted, as in our STM observations in case of the Fe/Cu system, is not surprising, particularly as the generation of defects in this system will be influenced by strains that are not only caused by pseudomorphic growth but are also due to the initial stages of transformation. After the dislocations are generated, the interface is semicoherent, and the dislocations can act as nucleation sites for further transformation processes, which is a well known effect controlling the growth of the product phase in martensitic transformations (e.g. cf. Refs. [37,39,40]).

A further interesting example of the interaction between misfit dislocations and bcc phase precipitations in the Fe/Cu system is reported in [28] where the tendency for some precipitates was observed to have boundaries coincident with the misfit dislocation lines. From the growth behaviour of such bcc precipitates, it could be concluded that the stress field on one side of the dislocations assisted the bcc transformation, whereas the stress field on the other side either inhibited it or was simply less favourable.

The observed complete absence of misfit disloca-

tions in the Fe/Ni system due to the relief of stress by contraction of the bcc precipitates along in-plane directions was already discussed in the previous section.

6. Summary

We have studied the effect of the reversal of applied strains on the fcc→bcc phase transformation in ultrathin iron films under UHV conditions. In the tensile-strained iron films on copper (100), the phase transformation starts by forming misfit dislocation-like ridge structures oriented along $\langle 011 \rangle$ directions at about 4.6 ML that soon develop into bcc phase precipitations with indications of a Pitsch orientation. Above 12 ML, the films are completely transformed into the bcc phase. During the transformation process, the appearance of the bcc precipitates in the Fe films does not disturb the layer-by-layer growth mode in the untransformed fcc region.

For the compressively strained iron films on nickel (100), no such dislocation-like structures have been observed during the whole growth. The transformation starts at about 5.5 ML by forming bcc island chains along $\langle 001 \rangle$ directions. The formation of the bcc islands results in a surface roughening process, and the growth mode of Fe on Ni changes from layer-by-layer to multilayer at about 6 ML. Above 10 ML, the bcc phase becomes dominant. In contrast to the Fe/Cu system, it is difficult to determine precisely the extent of the transformation in the Fe/Ni films, as easily distinguishable features between the transformed and untransformed regions are absent. The possibly relevant quantity is the density of the grooves that represent the gaps between two neighboring $\langle 001 \rangle$ oriented chains of bcc islands. These chains presumably decorate the sites of preferred nucleation that are formed by the periodic misfit strain maxima caused by the pseudomorphic growth of the first iron monolayers and occurring after exceeding a critical number of monolayers. During further growth, the particular geometry of the developing bcc islands is able to completely accommodate the misfit stresses and to make any misfit dislocations unnecessary in this system. The

maximum density of the grooves at 10 ML corresponds remarkably with the observed sharp rise in interlayer spacing at 10 ML.

The drastic differences between the observed transformation phenomena in the two systems are directly connected to the different sign of the strain acting in the films: They can be well understood if taking into account the specific possibilities of misfit accommodation in both systems and the effects of different applied stresses on the bcc precipitation kinetics.

References

- [1] V.L. Moruzzi, P.M. Markus, J. Kübler, *Phys. Rev. B* 39 (1989) 6957.
- [2] D.D. Chambliss, R.J. Wilson, S. Chiang, *J. Vac. Sci. Technol.* 4 (1992) 1993.
- [3] M.K. Kief, Egelhoff W.F., Jr, *Phys. Rev. B* 47 (1993) 10785.
- [4] M. Wuttig, J. Thomassen, *Surf. Sci.* 282 (1992) 237.
- [5] T. Detzel, N. Memmel, *Surf. Sci.* 293 (1993) 227.
- [6] J. Thomassen, B. Feldmann, M. Wuttig, *Surf. Sci.* 264 (1992) 406.
- [7] D.A. Steigerwald, Egelhoff W.F., Jr, *Surf. Sci.* 192 (1987) L887.
- [8] M. Arnot, E.M. McCash, W. Allison, *Surf. Sci.* 269/270 (1992) 724.
- [9] P. Dastoor, M. Arnot, E.M. McCash, W. Allison, *Surf. Sci.* 272 (1992) 154.
- [10] M. Wuttig, B. Feldmann, J. Thomassen, F. May, H. Zillgen, A. Brodde, H. Hannemann, H. Neddermeyer, *Surf. Sci.* 291 (1993) 14.
- [11] D.D. Chambliss, K. Johnson, K. Kalki, S. Chiang, R. Wilson, in: *Multilayers and Surfaces; Interfaces and Characterization*, MRS Symposia Proceedings No. 313, Materials Research Society, Pittsburgh, PA, 1993, p. 713.
- [12] K. Kalki, D.D. Chambliss, K.E. Johnson, R.J. Wilson, S. Chiang, *Phys. Rev. B* 48 (1993) 18344.
- [13] A.K. Schmidt, J. Kirschner, *J. Vac. Sci. Technol. B* 9 (1991) 649.
- [14] J. Giergiel, J. Kirschner, J. Landgraf, J. Shen, J. Woltersdorf, *Surf. Sci.* 310 (1994) 1.
- [15] J. Giergiel, J. Shen, J. Woltersdorf, A. Kirilyuk, J. Kirschner, *Phys. Rev. B* 52 (1995) 8528.
- [16] G.A. Prinz, *J. Magn. Mater.* 100 (1991) 469.
- [17] K.S. Cheung, R.J. Harrison, *J. Appl. Phys.* 71 (1992) 4009.
- [18] A.K. Schmid, J. Kirschner, *J. Vac. Sci. Technol. B* 9 (1991) 649.
- [19] S.H. Lu, Z.Q. Wang, D. Tian, Y.S. Li, F. Jona, *Surf. Sci.* 221 (1989) 35.
- [20] M. Albrecht, H. Fritzsche, U. Gradmann, *Surf. Sci.* 294 (1993) 1.

- [21] M.J. Bibby, J.G. Parr, *J. Iron Steel Inst.* 202 (1964) 100.
- [22] J.D. Watson, P.G. McDougall, *Acta Met.* 21 (1973) 961.
- [23] H. Schumann, *Crystal Geometry: Theory of Lattice Transformations*, DVG, Leipzig, 1980.
- [24] J.H. van der Merwe, J. Woltersdorf, W.A. Jesser, *Mater. Sci. Eng.* 81 (1986) 1.
- [25] J. Woltersdorf, *Thin Solid Films* 85 (1981) 241.
- [26] W.A. Jesser, J.W. Matthews, *Phil. Mag.* 15 (1967) 1097.
- [27] J.W. Matthews, W.A. Jesser, *Phil. Mag.* 20 (1969) 999.
- [28] G.H. Olsen, W.A. Jesser, *Acta Met.* 19 (1971) 1009.
- [29] G.H. Olsen, W.A. Jesser, *Acta Met.* 19 (1971) 1299.
- [30] J.D. Eshelby, *Elastic inclusions and inhomogeneities* in: I.N. Sneddon, R. Hill (Eds.), *Progress in Solid Mechanics*, Vol. II, North Holland, Amsterdam, 1961, p. 89.
- [31] E.C. Bain, *Trans. Am. Inst. Min. Eng.* 70 (1924) 25.
- [32] J.W. Christian, *The Theory of Transformations in Metals and Alloys*, Pergamon Press, Oxford, 1965.
- [33] C.M. Wayman, *Introduction to the Crystallography of Martensitic Transformations*, Macmillan, London, 1964.
- [34] Z. Nishiyama, *Rep. Res. Inst. Tohoku Univ.* 23 (1934) 637.
- [35] G. Kurdjumow, G. Sachs, *Z. Physik* 64 (1934) 325.
- [36] W. Pitsch, *Phil. Mag.* 4 (1959) 577.
- [37] G. Guenin, P.F. Gobin, *Proc. Int. Conf. Martens. Transform. ICOMAT 79*, 1979, p. 532.
- [38] J.W. Matthews, in: J.W. Matthews (Ed.), *Epitaxial Growth, Part B*, Academic Press, New York, 1975, p. 560.
- [39] G.B. Olsen, M. Cohen, *J. Phys. C* 43 (1982) 75.
- [40] T. Suzuki, M. Wuttig, *Acta Met.* 23 (1975) 1069.